Efficient Photocatalytic Hydrogen Evolution by Iron Platinum Loaded Reduced Graphene Oxide

doi: 10.15255/CABEQ.2015.2222

S. E. Moradi*
Young Researchers and Elite Club, Islamic Azad University-Sari Branch, Sari, Iran

Original scientific paper
Received: April 28, 2015
Accepted: February 23, 2016

In this work, graphene oxide (GO) was prepared by the Hummers method from natural graphite, and modified with iron and platinum nanoparticles by the solvothermal method. The structural order and textural properties of the grapheme-based materials were studied by BET, TEM, XRD, TG-DTA, and XPS techniques. UV−Vis diffuse reflectance spectra indicate the band gap for FePt and FePt-rGO composites to be 3.2 and 2.8 eV, respectively. FePt-rGO showed a hydrogen generation rate higher than that of the FePt nanoparticles. A detailed study of Pt effect on the photocatalytic H_2 production rates showed that Pt NPs could act as an effective co-catalyst, enhancing photocatalytic activity of FePt-rGO. The FePt-rGO gave a H_2 production rate of 125 μmol g^{-1} h^{-1}. This is ascribed to the presence of Pt NPs (acting as electron sinks) and graphene oxide (as an electron collector and transporter) in FePt-rGO composites.

Key words:
hydrogen evolution, reduced graphene oxide, photocatalysis, platinum nanoparticle, iron nanoparticle

Introduction

The production of hydrogen (as a clean energy carrier that could replace fossil fuels) nowadays attracts much attention because of environmental pollution and energy demands[1–3]. Recently, hydrogen evolution technologies, such as production by steam reforming[4], electrolysis[5], degradation of organic pollutants in wastewater[6], and photoelectrochemical splitting of water[7] have been investigated. Among all the methods, photocatalytic hydrogen generation processes[8–10] on nanomaterials have gained considerable attention because of their ability to provide a clean and renewable energy source.

Photocatalytic splitting of water promises to be a cleaner and greener route towards generation of hydrogen. A key challenge for water splitting is the development of catalysts for the direct and efficient production of hydrogen from protons. Up to now, numerous metal-based photocatalysts have been discovered as catalysts for this reaction[11,12], but they are ultimately of low efficiency, high cost, and low abundance[13,14]. Several strategies have been employed to improve the photocatalytic performance of metallic photocatalysts, for example, textural design[15,16], coupling with other metal photocatalysts[17,18], etc. In particular, great interest has been devoted to linking carbon nanomaterials[19]. Conjugated carbon materials, such as fullerenes, graphene, carbon nanotubes, and graphite are excellent candidates for refining the transport of photocarriers during photocatalysis through the formation of electronic interactions with photocatalyst nanoparticles. Among carbon-based materials, graphene has been reported as an efficient co-catalyst for photocatalytic H_2 production because of its high specific surface area (theoretical value 2600 m^2 g^{-1}), excellent electron mobility (15000 m^2 V^{-1} s^{-1} at room temperature), thermal conductivity, and high mechanical strength[20–22]. In recent years, reduced graphene oxide (rGO) has been modified with different nanoparticles, such as ZnO[23], TiO_2[24] and CdS[25]. They have been used as photocatalysts under visible-light irradiation. Previously, a few shape-controlled Pt alloy nanocrystals, such as Pt-Fe and Pt-Co[26], have been made using diols and other reducing agents. To the best of our knowledge, metals like Pt and Fe play a significant role in the hydrogen evolution process, especially when they are combined with carbon-based composites[27–30].

Herein, we have attempted to introduce the grapheme-based composite as a novel class of photocatalysts for enhancement of photocatalytic hydrogen evolution. In this work, we have synthesized platinum-iron NPs loaded reduced graphene oxide using $Pt(acac)_2$ and $Fe(acac)_3$ as metal nanoparticle sources. We have also examined the photocatalytic activity of FePt-rGO and FePt nanomaterials for the water splitting reaction to produce hydrogen in the presence of methanol as a sacrificial agent.

*Corresponding author: Seyyed Ershad Moradi,
e-mail: er_moradi@hotmail.com; Tel.: 98-11-33314785

Experimental

Materials

Graphite powder (<20 micron) was purchased from Sigma-Aldrich (St. Louis, MO, USA) and used as received. H_2SO_4 (>99 %), hydrochloric acid (AR grade), H_2O_2 (30 % (w v^{-1})), $KMnO_4$ (>99 %), Platinum acetylacetonate ($Pt(acac)_2$, 97 %)), iron acetylacetonate ($Fe(acac)_3$, 99.9 %), and ethylene glycol (EG) were all purchased from Sigma-Aldrich (St. Louis, MO, USA).

Synthesis of GO adsorbent

GO was synthesized from expandable graphite using a modified Hummers' method[31]. An amount of 1 g of graphite powder was added to 23 mL of concentrated H_2SO_4 in an ice bath. $KMnO_4$ (3 g) was then added slowly with stirring and cooling to keep the temperature of the reaction mixture below 293 K. The temperature of the reaction mixture was increased and maintained at 308 K for 30 minutes. When 46 mL of deionized water was added slowly to this mixture, the temperature was increased to 371 K. After 15 minutes, 140 mL of deionized water was added followed by 10 mL of 30 % H_2O_2 solution. The solid product was separated by centrifugation. It was washed repeatedly with 5 % HCl solution until the sulfate ions had been removed, and then washed with distilled water repeatedly until free of chloride ions. The product was then filtered and washed 3–4 times with acetone to make it moisture-free, and the residue dried in an oven at 338 K overnight. The GO was suspended in water and exfoliated by ultrasonication for 3 hours.

Synthesis of FePt-rGO composites

FePt-rGO was obtained by the method as described by Chen *et al.*[32] Prior to the synthesis of FePt-rGO, the as-prepared GO was dispersed in deionized water by ultrasonication (KQ-50B supersonic cleaner, Kun Shan Ultrasonic Instruments Co., Ltd, China; ultrasonic frequency: 40 kHz; ultrasonic power: 80W) for 3 hours. FePt-rGO composites were synthesized by the solvothermal method using ethylene glycol (EG)–water as the solvent. In a typical synthesis, $Pt(acac)_2$ (0.25 mmol, 0.0985 g) was dissolved in EG (15 mL) under magnetic stirring with a short heating (90–100 °C, 5 min). $Fe(acac)_3$ (0.25 mmol, 0.0883 g) was dissolved in another 15 mL of EG under magnetic stirring with a short heating period (below 100 °C), which was subsequently added dropwise into the EG solution containing $Pt(acac)_2$. Then, 10 mL of GO (5 mg mL^{-1}) aqueous dispersion was added dropwise into the EG solution. After 30 minutes of stirring, the mixture was transferred to, and sealed in, a 50-mL Teflon-lined stainless steel autoclave, and heated to 160 °C for 24 h, and then cooled to room temperature. The precipitate was collected and washed alternately with ethanol and deionized water by centrifugation (10,000 rpm, 5 min), and then dried at 60 °C in vacuum.

Characterization and hydrogen evolution

The morphology and surface structure of GO and FePt-rGO were examined by X-ray diffraction (XRD, Philips Xpert MPD, Co Kα irradiation, λ = 1.78897 A°), and the X-ray photoemission spectroscopy (XPS) analysis was acquired by using a Scienta ESCA 200 analyzer (Gammadata, Sweden) equipped with a monochromatized Al Ka X-ray source. Transmission electron microscope (TEM) analysis was conducted with a JEM 2100 transmission electron microscope (JEOL, Japan) at 200 kV. The composition and thermal properties of GO and FePt-rGO were determined by TGA with a PL Thermal Sciences; model PL-STA using a heating rate of 10 K min^{-1} from room temperature to 1073 K. The measurements were conducted using approximately 3-mg samples, and then weight retention/temperature curves were recorded.

Volumetric nitrogen sorption studies were taken at 77 K using a Micromeritics ASAP 2020 system. Before performing the measurements, the samples were degassed below 1.33 Pa at 90 °C for 1 h and heated (10 °C min^{-1}) to 350 °C for 10 h. The specific surface area (SBET) was calculated by the BET method in the relative pressure range of 0.04–0.20. Total pore volume (V_t) was calculated at relative pressure p/p_0 = 0.98. The microporous volume (V_{mi}) was determined by applying Dubinin–Radushkevich (DR) analyses on the corresponding isotherms in the relative pressure range 10^{-4}–10^{-2}. The volume of pores smaller than 1 nm (V < 1 nm) was determined by the cumulative pore volume in the relative pressure range 10^{-6}–10^{-4} using the Horvath–Kawazoe (HK) method. The meso- and micropore sizes of samples were analyzed by the Barrett–Joyner–Halenda (BJH) and HK methods, respectively. A Shimadzu spectrophotometer (Model 2501 PC) was used to record the UV-Vis diffuse reflectance spectra of the samples with the region of 200 to 800 nm.

The photocatalytic hydrogen evolution tests were carried out at room temperature under atmospheric pressure in a closed quartz reactor system. The light intensity was measured to be 80 mW cm^{-2} by an optical power meter (1 L, 1400 A, International Light) from a 400 W high-pressure Hg lamp with a water filter to remove the infrared part of the spectrum. Typically, the photocatalysts (5 mg) were suspended in an aqueous methanol solution (80 mL

of distilled water, 20 mL of methanol) by means of a magnetic stirrer within the reactor. Prior to the experiment, the mixture was dispersed by ultrasound treatment for 15 minutes, followed by purging N_2 gas for 30 minutes. The amount of evolved H_2 was determined by a GC5890F gas chromatograph (thermal conductivity detector, molecular sieve 5A, 99.999 % N_2 carrier).

Results and discussion

Characterization of the GO and FePt-rGO samples

Fig. 1 shows the nitrogen adsorption–desorption isotherms of GO and FePt-rGO, which were used to investigate the surface area and porous structure. The surface area of GO and FePt-rGO calculated by the Brunauer–Emmett–Teller (BET) theory, which explain the physical adsorption of gas molecules on a solid surface[33], are 741.2 and 1018.7 $m^2\ g^{-1}$, respectively.

As shown in Fig. 2a, the broad and relatively weak diffraction peak at $2\theta = 10.5°$ ($d = 0.87$ nm), which corresponds to the typical diffraction peak of graphene oxide adsorbent, is attributed to the (002) plane[34]. The 2θ values for FePt-rGO at 40.77°, 46.92°, 69.30°, and 83.10° can be indexed to diffraction planes of (111), (200), (220), and (311), respectively. The mentioned planes can be attributed to chemically disordered fcc metal nanoparticle[12]. No peaks from the iron oxides were observed in the XRD data, confirming that the iron nanoparticles were not oxidized. The peak at ca. 24.32° (2θ) is related to carbon peak of reduced graphene oxide[35].

A representative TEM image of the obtained FePt-rGO is shown in Fig. 3a. The TEM image of FePt-rGO also shows that platinum-iron nanoparticles are relatively well-dispersed on the reduced graphene oxide sheet. The mean size of FePt-rGO

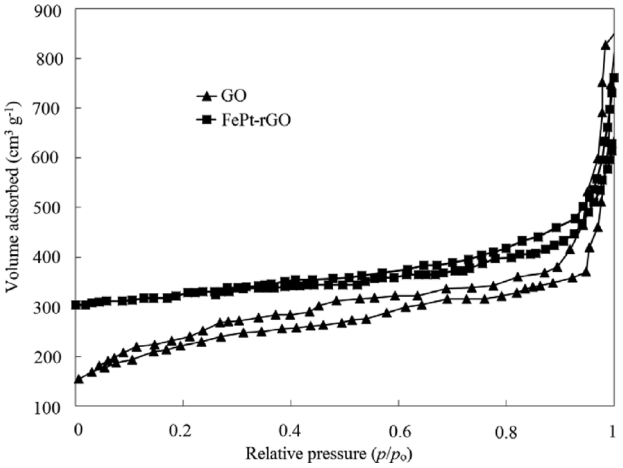

Fig. 1 – *Nitrogen adsorption–desorption isotherms of GO and FePt-rGO*

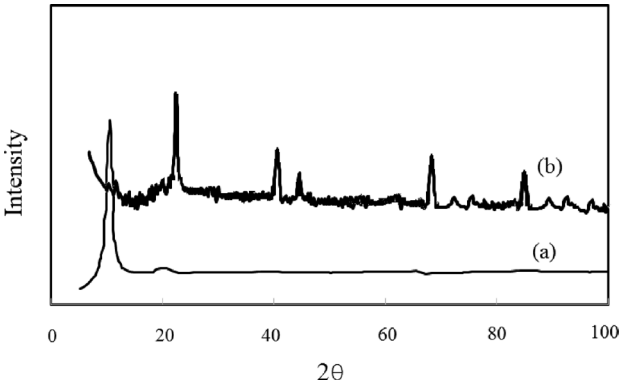

Fig. 2 – *XRD pattern of (a) GO and (b) FePt-rGO*

calculated from the TEM image is around 16.0 nm. The histogram of particle size for FePt-rGO show that the size distribution is relatively narrow (Fig. 3b).

Fig. 4 displays Pt 4f and Fe 2p X-ray photoelectron spectroscopy (XPS) spectra of FePt-rGO composites. The two characteristic peaks at 71.3 eV (Pt $4f_{7/2}$) and 74.5 eV (Pt $4f_{5/2}$) may be observed in

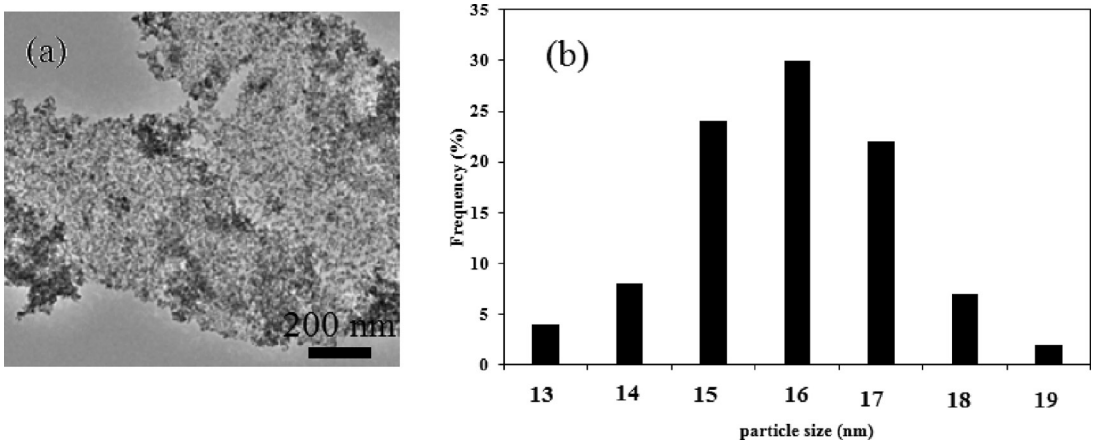

Fig. 3 – *(a) TEM photographs, and (b) histogram of particle size distribution of FePt-rGO*

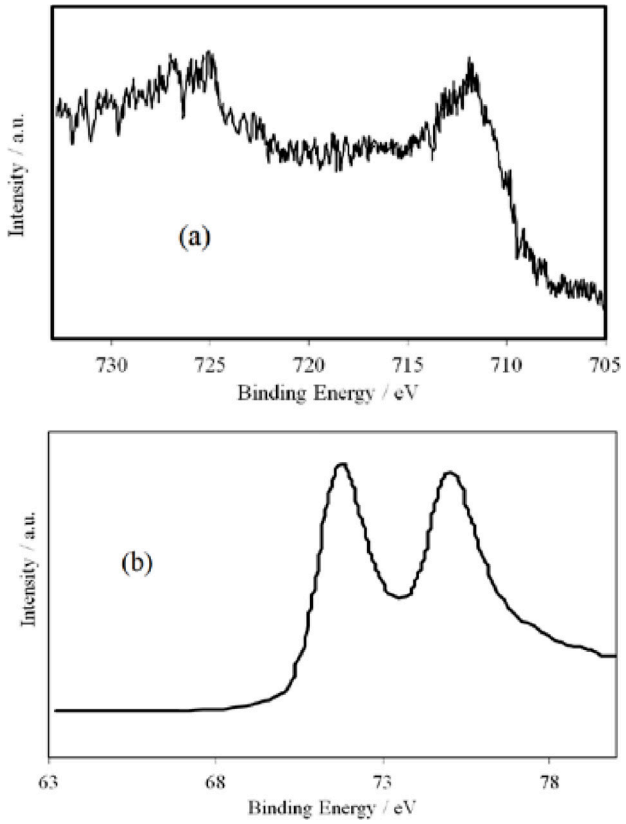

Fig. 4 – *XPS spectra of Fe 2p in the FePt-rGO composites and (b) XPS spectra of Pt 4f in the FePt-rGO composites*

Fig. 4a, confirming the formation of metallic Pt. The peaks at 711.1 eV ($Fe2p_{3/2}$) and 725.6 eV ($Fe\ 2p_{1/2}$) presented in Fig. 4b, show the existence of Fe-O or Fe-OOH group in FePt-rGO composites. Moreover, no signal for the C in the XPS is provided, which would be useful to confirm the reduction of GO.

The TGA was also performed on GO and the FePt-rGO samples to determine the structure and thermal stability of the GO and the FePt-rGO (Fig. 5a and Fig. 5b). GO shows two significant weight losses close to 100 °C and 500 °C with 9 % and 30 % weight loss, respectively. They are related to the evaporation of the water molecules in the material and thermal decomposition of oxygen carrying functionalities and oxidation of carbon. The FePt-rGO shows a 2 % loss below 100 °C which should be due to the removal of adsorbed water, a 3 % loss at ca. 200 °C should be assigned to the decomposition of the residual oxygen containing groups, and a 13 % loss from 440 to 590 °C should be associated with the pyrolysis of the carbon skeleton of reduced graphene oxide[36]. These results suggest that FePt-rGO is thermally stable at higher temperatures.

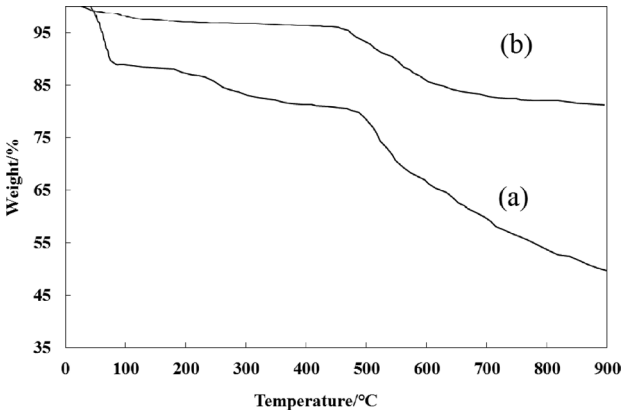

Fig. 5 – *TGA curves of (a) GO and (b) FePt-rGO*

To investigate the optical properties, UV-Vis absorption spectra of FePt and FePt-rGO are shown in Fig. 6. It can be observed that FePt and FePt-rGO show sharp absorption edges at around 470 nm. Fig. 6b displays the plot of the transformed Kubelka-Munk function versus energy of light, by which the estimated band gaps are 3.2 and 2.8 eV, corresponding to FePt and FePt-rGO, respectively. The narrow band gap of FePt-rGO nanoparticles was attributed to the interaction between rGO and FePt.

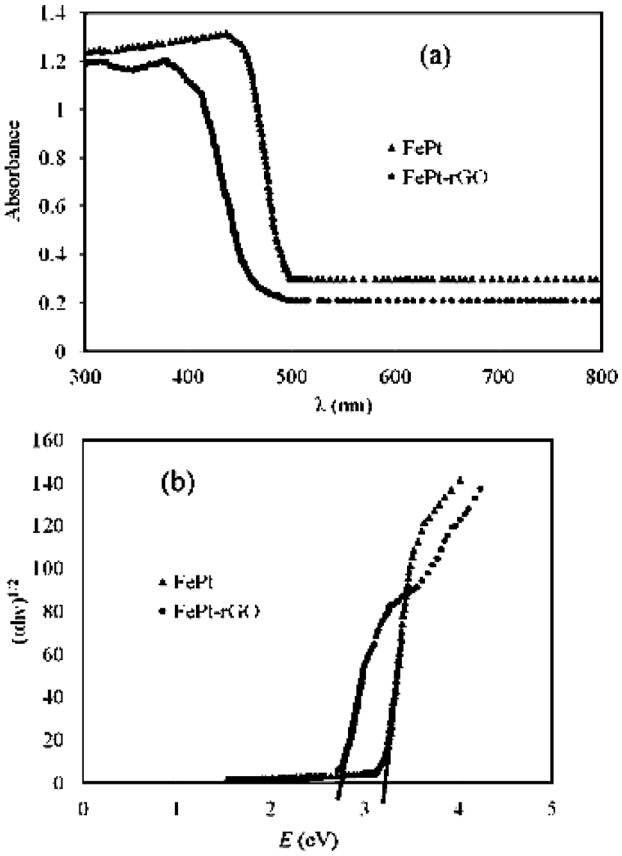

Fig. 6 – *(a) UV-Vis diffuse reflectance spectra of FePt and FePt-rGO nanoparticles (b) corresponding plot of transformed Kubelka-Munk function versus the energy of the light absorbed*

Photocatalytic hydrogen evolution activity and mechanism

The hydrogen generating capability of the composite photocatalysts was investigated in methanol aqueous solution. The photocatalytic results of the reduction of water to produce H_2 over FePt and FePt-rGO catalysts are shown in Fig. 7. The rate of hydrogen evolution continuously increased at the initial reaction duration, and after several hours, it reached a constant value of 125 μmol g^{-1} h^{-1} (Fig. 7). The total amount of H_2 evolved from FePt-rGO after 6 h of irradiation was 890 μmol g^{-1}, which was higher than that of FePt (460 μmol g^{-1}). The higher photocatalytic activity might be attributable to good light absorption of FePt-rGO compared to FePt NPs. It is reasonable to imagine the formation of a Schottky-like barrier between the closely contacted iron and platinum NPs surface species, which would facilitate electron–hole separation, similar to the action of traditional conductive platinum co-catalysts[37].

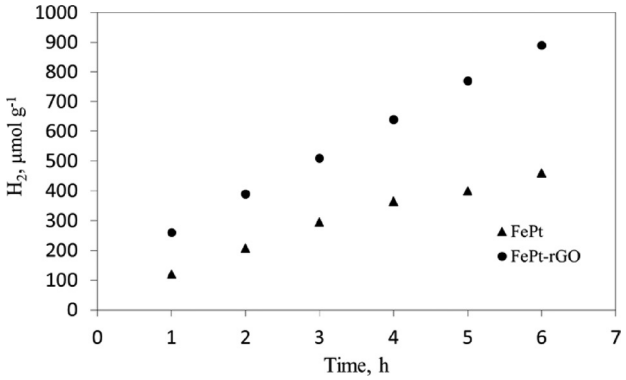

Fig. 7 – *Amount of hydrogen gas produced by (a) FePt-rGO and (b) FePt NPs (Reaction conditions: $m_{catalyst}$ = 5 mg, [methanol] = 10 wt %, pH = 7, T = 25 °C)*

The highest rates of H_2 generation with the above amounts of nanomaterials are shown in Fig. 7. We can see a drastic increase in the amount of evolved H_2 gas when FePt is used with reduced graphene oxide. This is due to the synergy effect of rGO to FePt. In the case of noble metal, such as Pt, an electron from photoexcited iron oxide is transferred to Pt, and then it reduces H^+ ion to produce H_2 gas. Platinum nanoparticles loaded on the rGO surface are known to act as electron sinks. This strongly enhances the photocatalytic activity of iron oxide through the formation of a Schottky barrier (retarding the electron/hole recombination) at the FePt-rGO surface. This phenomenon appears to promote an efficient separation of holes and electrons charges carriers photo-generated under near-UV light. As a result, the interfacial charge transfer and the efficiency of the photocatalytic reaction are enhanced[38–40]. Platinum deposits can serve as a temporary electron chamber.

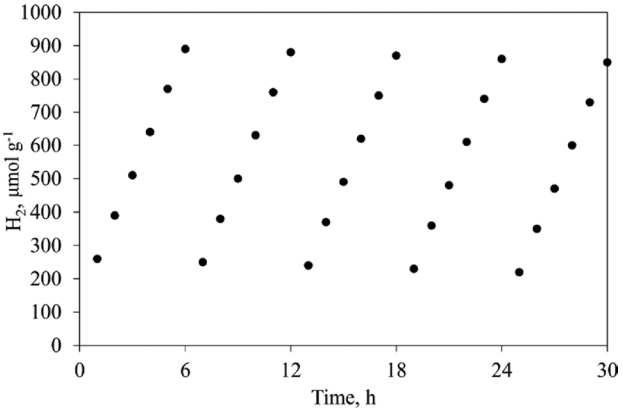

Fig. 8 – *Photocatalytic H_2 evolution on FePt-rGO photocatalysts with intermittent evacuation every 6 h*

Fig. 8 shows the hydrogen evolution by recycled FePt-rGO. After each cycle, the amount of hydrogen evolution from FePt-rGO remained constant. Fig. 8 shows that the photocatalytic evolution rate of hydrogen remained above 95 % of the initial rate. After 30 h of irradiation, the system produced 850 μmol g^{-1} of H_2 without noticeable catalyst deactivation.

Conclusion

Hydrogen evolution from water containing methanol was performed on FePt-rGO by medium-pressure Hg lamp. XPS analysis confirmed that Fe and Pt species were coordinated to reduced graphene oxides. Diffuse reflectance spectra revealed an increase in absorption with Fe and Pt NPs implying that the doping modified the electronic properties of reduced graphene oxide. The significant promotion effect of hydrogen evolution using FePt-loaded reduced graphene oxide photocatalysts was observed. The Pt and Fe NPs enhance the photocatalytic hydrogen evolution activity of FePt-rGO. The hydrogen evolution of FePt-rGO was 125 μmol g^{-1} h^{-1} with a maximum of 890 μmol g^{-1}, which exceeded 1.9 times compared with FePt NPs.

ACKNOWLEDGMENTS

The author thanks The Research Council at the Azad University for financial support.

References

1. *Teets, T. S., Nocera, D. G.,* Photocatalytic Hydrogen Production, Chem. Commun. **47** (2011) 9268. doi: http://dx.doi.org/10.1039/c1cc12390d
2. *Leygraf, C., Hendewerk, M., Somorjai, G. A.,* Photocatalytic Production of Hydrogen from Water by a P- and N-Type Polycrystalline Iron Oxide Assembly, J. Phys. Chem. **86** (1982) 4484. doi: http://dx.doi.org/10.1021/j100220a007

3. *Xing, C., Zhang, Y., Yan, W., Guo, L.,* Band Structure-Controlled Solid Solution of Photocatalyst for Hydrogen Production by Water Splitting, Int. J. Hydrogen Energy **31** (2006) 2018.
doi: http://dx.doi.org/10.1016/j.ijhydene.2006.02.003
4. *Yu, D., Aihara, M., Antal, M. J.,* Hydrogen Production by Steam Reforming Glucose in Supercritical Water, Energy Fuels **7** (1993) 574.
doi: http://dx.doi.org/10.1021/ef00041a002
5. *Barbir, F.,* PEM Electrolysis for Production of Hydrogen from Renewable Energy Sources, Sol. Energ. **78** (2005) 661.
doi: http://dx.doi.org/10.1016/j.solener.2004.09.003
6. *Kim, J., Monllor-Satoca, D., Choi, W.,* Simultaneous Production of Hydrogen with the Degradation of Organic Pollutants Using TiO_2 Photocatalyst Modified with Dual Surface Components, Energy. Environ. Sci. **5** (2012) 7647.
doi: http://dx.doi.org/10.1039/c2ee21310a
7. *Sathre, R., Scown, C. D., Morrow, W. R., Stevens, J. C., Sharp, I. D., Ager, J. W., Walczak, K., Houle, F. A., Greenblatt, J. B.,* Life-Cycle Net Energy Assessment of Large-Scale Hydrogen Production Via Photoelectrochemical Water Splitting, Energy. Environ. Sci. **7** (2014) 3264.
doi: http://dx.doi.org/10.1039/C4EE01019A
8. *Lingampalli, S. R., Gautam, U. K., Rao, C. N. R.,* Highly Efficient Photocatalytic Hydrogen Generation by Solution-Processed ZnO/Pt/CdS, ZnO/Pt/Cd1-xZnxS and ZnO/Pt/CdS1-xSex Hybrid Nanostructures, Energy Environ. Sci. **6** (2013) 3589.
doi: http://dx.doi.org/10.1039/c3ee42623h
9. *Natali, M., Luisa, A., Iengo, E., Scandola, F.,* Efficient Photocatalytic Hydrogen Generation from Water by a Cationic Cobalt(Ii) Porphyrin, Chem. Commun. **50** (2014) 1842.
doi: http://dx.doi.org/10.1039/c3cc48882a
10. *Jing, D., Guo, L., Zhao, L., Zhang, X., Liu, H., Li, M., Shen, S., Liu, G., Hu, X., Zhang, X., Zhang, K., Ma, L., Guo, P.,* Efficient Solar Hydrogen Production by Photocatalytic Water Splitting: From Fundamental Study to Pilot Demonstration, Int. J. Hydrogen Energy **35** (2010) 7087.
doi: http://dx.doi.org/10.1016/j.ijhydene.2010.01.030
11. *Ni, M., Leung, M. K. H., Leung, D. Y. C., Sumathy, K.,* A Review and Recent Developments in Photocatalytic Water-Splitting Using for Hydrogen Production, Renew. Sustainable Energy Rev. **11** (2007) 401.
doi: http://dx.doi.org/10.1016/j.rser.2005.01.009
12. *Zhang, J., Yang, H., Yang, K., Fang, J., Zou, S., Luo, Z., Wang, H., Bae, I.-T., Jung, D. Y.,* 'Monodisperse Pt_3Fe Nanocubes: Synthesis, Characterization, Self-Assembly, and Electrocatalytic Activity', Adv. Funct. Mater. **20** (2010) 3727.
doi: http://dx.doi.org/10.1002/adfm.201000679
13. *Chen, X., Shen, S., Guo, L. Mao, S. S.*, Semiconductor-Based Photocatalytic Hydrogen Generation, Chem. Rev. **110** (2010) 6503.
doi: http://dx.doi.org/10.1021/cr1001645
14. *Aharon-Shalom, E., Heller, A.,* Efficient p - InP(Rh - H alloy) and p - InP(Re - H alloy) Hydrogen Evolving Photocathodes, J. Electrochem. Soc. **129** (1982) 2865.
doi: http://dx.doi.org/10.1149/1.2123695
15. *Gadiou, R., Saadallah, S.-E., Piquero, T., David, P., Parmentier, J., Vix-Guterl, C.,* The Influence of Textural Properties on the Adsorption of Hydrogen on Ordered Nanostructured Carbons, Microporous Mesoporous Mater. **79** (2005) 121.
doi: http://dx.doi.org/10.1016/j.micromeso.2004.10.034
16. *Armandi, M., Bonelli, B., Otero Areán, C., Garrone, E.,* Role of Microporosity in Hydrogen Adsorption on Templated Nanoporous Carbons, Microporous Mesoporous Mater. **112** (2008) 411.
doi: http://dx.doi.org/10.1016/j.micromeso.2007.10.017
17. *Nguyen, N. T., Yoo, J., Altomare, M., Schmuki, P.,* 'Suspended" Pt Nanoparticles over TiO_2 Nanotubes for Enhanced Photocatalytic H_2 Evolution, Chem. Commun. **50** (2014) 9653.
doi: http://dx.doi.org/10.1039/C4CC04087B
18. *Zhu, Y., Ling, Q., Liu, Y., Wang, H., Zhu, Y.,* Photocatalytic H_2 Evolution on MoS_2-TiO_2 Catalysts Synthesized Via Mechanochemistry, Phys. Chem. Chem. Phys. **17** (2015) 933.
doi: http://dx.doi.org/10.1039/C4CP04628E
19. *Inagaki, M., Kojin, F., Tryba, B., Toyoda, M.,* Carbon-Coated Anatase: The Role of the Carbon Layer for Photocatalytic Performance, Carbon **43** (2005) 1652.
doi: http://dx.doi.org/10.1016/j.carbon.2005.01.043
20. *Mukherji, A., Seger, B., Lu, G. Q., Wang, L.,* Nitrogen Doped $Sr_2Ta_2O_7$ Coupled with Graphene Sheets as Photocatalysts for Increased Photocatalytic Hydrogen Production, ACS Nano **5** (2011) 3483.
doi: http://dx.doi.org/10.1021/nn102469e
21. *Wang, H., Yuan, X., Wu, Y., Huang, H., Peng, X., Zeng, G., Zhong, H., Liang, J., Ren, M. M.,* Graphene-Based Materials: Fabrication, Characterization and Application for the Decontamination of Wastewater and Wastegas and Hydrogen Storage/Generation, Adv. Colloid Interface Sci. **195-196** (2013) 19.
doi: http://dx.doi.org/10.1016/j.cis.2013.03.009
22. *Shin, H.-J., Choi, W. M., Choi, D., Han, G. H., Yoon, S.-M., Park, H.-K., Kim, S.-W., Jin, Y. W., Lee, S. Y., Kim, J. M., Choi, J.-Y., Lee, Y. H.,* Control of Electronic Structure of Graphene by Various Dopants and Their Effects on a Nanogenerator, J. Am. Chem. Soc. **132** (2010) 15603.
doi: http://dx.doi.org/10.1021/ja105140e
23. *Rajesh, U. C., Wang, J., Prescott, S., Tsuzuki, T., Rawat, D. S.,* rGO/ZnO Nanocomposite: An Efficient, Sustainable, Heterogeneous, Amphiphilic Catalyst for Synthesis of 3-Substituted Indoles in Water, ACS Sustainable Chem. Eng. **3** (2014) 9.
doi: http://dx.doi.org/10.1021/sc500594w
24. *Qu, Y., Gao, Y., Kong, F., Zhang, S., Du, L., Yin, G.*, Pt–RGO–TiO_2 Nanocomposite by Uv-Photoreduction Method as Promising Electrocatalyst for Methanol Oxidation, Int. J. Hydrogen Energy **38** (2013) 12310.
doi: http://dx.doi.org/10.1016/j.ijhydene.2013.07.038
25. *Li, P., Zhou, Y., Li, H., Xu, Q., Meng, X., Wang, X., Xiao, M., Zou, Z.,* All-Solid-State Z-Scheme System Arrays of $Fe_2v_4o_{13}$/Rgo/Cds for Visible Light-Driving Photocatalytic CO_2 Reduction into Renewable Hydrocarbon Fuel, Chem. Commun. **51** (2015) 800.
doi: http://dx.doi.org/10.1039/C4CC08744E
26. *Li, J., Wang, G., Wang, J., Miao, S., Wei, M., Yang, F., Yu, L., Bao, X.,* Architecture of PtFe/C Catalyst with High Activity and Durability for Oxygen Reduction Reaction, Nano Res. **7** (2014) 1519.
doi: http://dx.doi.org/10.1007/s12274-014-0513-0
27. *Thoi, V. S., Usiskin, R. E., Haile, S. M.,* Platinum-Decorated Carbon Nanotubes for Hydrogen Oxidation and Proton Reduction in Solid Acid Electrochemical Cells, Chem. Sci. **6** (2015) 1570.
doi: http://dx.doi.org/10.1039/C4SC03003F
28. *Kuyunko, N. S., Kushch, S. D., Muradyan, V. E., Volodin, A. A., Torbov, V. I., Tarasov, B. P.,* Pt Nanoclusters on Carbon Nanomaterials for Hydrogen Fuel Cells, in Hydrogen Materials Science and Chemistry of Carbon Nanomaterials, Springer Netherlands, 2007, pp. 213-18.
doi: http://dx.doi.org/10.1007/978-1-4020-5514-0_26

29. *Wakabayashi, N., Takeichi, M., Uchida, H., Watanabe, M.,* Temperature Dependence of Oxygen Reduction Activity at Pt−Fe, Pt−Co, and Pt−Ni Alloy Electrodes, J. Phys. Chem. B **109** (2005) 5836.
doi: http://dx.doi.org/10.1021/jp046204+
30. *Sumida, K., Horike, S., Kaye, S. S., Herm, Z. R., Queen, W. L., Brown, C. M., Grandjean, F., Long, G. J., Dailly, A., Long, J. R.,* Hydrogen Storage and Carbon Dioxide Capture in an Iron-Based Sodalite-Type Metal-Organic Framework (Fe-BTT) Discovered Via High-Throughput Methods, Chem. Sci. **1** (2010) 184.
doi: http://dx.doi.org/10.1039/c0sc00179a
31. *Hummers, W. S., Offeman, R. E.,* Preparation of Graphitic Oxide, J. Am. Chem. Soc. **80** (1958) 1339.
doi: http://dx.doi.org/10.1021/ja01539a017
32. *Chen, D., Zhao, X., Chen, S., Li, H., Fu, X., Wu, Q., Li, S., Li, Y., Su, B.-L., Ruoff, R. S.,* One-Pot Fabrication of FePt/Reduced Graphene Oxide Composites as Highly Active and Stable Electrocatalysts for the Oxygen Reduction Reaction, Carbon **68** (2014) 755.
doi: http://dx.doi.org/10.1016/j.carbon.2013.11.064
33. *Brunauer, S., Emmett, P. H., Teller, E.,* Adsorption of Gases in Multimolecular Layers, J. Am. Chem. Soc. **60** (1938) 309.
doi: http://dx.doi.org/10.1021/ja01269a023
34. *Zhu, Y., Stoller, M. D., Cai, W., Velamakanni, A., Piner, R. D., Chen, D., Ruoff, R. S.,* Exfoliation of Graphite Oxide in Propylene Carbonate and Thermal Reduction of the Resulting Graphene Oxide Platelets, ACS Nano. **4** (2010) 1227.
doi: http://dx.doi.org/10.1021/nn901689k
35. *Qiu, J.-D., Wang, G.-C., Liang, R.-P., Xia, X.-H., Yu, H.-W.,* Controllable Deposition of Platinum Nanoparticles on Graphene as an Electrocatalyst for Direct Methanol Fuel Cells, J. Phys. Chem. C. **115** (2011) 15639.
doi: http://dx.doi.org/10.1021/jp200580u
36. *Liu, J., Tao, L., Yang, W., Li, D., Boyer, C., Wuhrer, R., Braet, F., Davis, T. P.,* Synthesis, Characterization, and Multilayer Assembly of pH Sensitive Graphene−Polymer Nanocomposites, Langmuir **26** (2010) 10068.
doi: http://dx.doi.org/10.1021/la1001978
37. *Williams, P. A., Ireland, C. P., King, P. J., Chater, P. A., Boldrin, P., Palgrave, R. G., Claridge, J. B., Darwent, J. R., Chalker, P. R., Rosseinsky, M. J.,* Atomic Layer Deposition of Anatase TiO_2 Coating on Silica Particles: Growth, Characterization and Evaluation as Photocatalysts for Methyl Orange Degradation and Hydrogen Production, J. Mater. Chem. **22** (2012) 20203.
doi: http://dx.doi.org/10.1039/c2jm33446a
38. *Kandiel, T. A., Dillert, R., Bahnemann, D. W.,* Enhanced Photocatalytic Production of Molecular Hydrogen on TiO_2 Modified with Pt-Polypyrrole Nanocomposites, Photochem. Photobiol. Sci. **8** (2009) 683.
doi: http://dx.doi.org/10.1039/b817456c
39. *Riassetto, D., Holtzinger, C., Messaoud, M., Briche, S., Berthomé, G., Roussel, F., Rapenne, L., Langlet, M.,* Mechanisms Involved in the Platinization of Sol–Gel-Derived TiO_2 Thin Films, J. Photochem. Photobiol. A. **202** (2009) 214.
doi: http://dx.doi.org/10.1016/j.jphotochem.2008.11.023
40. *Lee, J., Choi, W.,* Photocatalytic Reactivity of Surface Platinized TiO_2: Substrate Specificity and the Effect of Pt Oxidation State, J. Phys. Chem. B **109** (2005) 7399.
doi: http://dx.doi.org/10.1021/jp044425+